J. Fluid Mech. (1971), *vol.* 48, *part* 1, *pp.* 41–71
Printed in Great Britain

Some measurements of particle velocity autocorrelation functions in a turbulent flow

By W. H. SNYDER† AND J. L. LUMLEY
The Pennsylvania State University, University Park, Pennsylvania

(Received 29 June 1970)

Particle velocity autocorrelations of single spherical beads (46·5 μ hollow glass, 87 μ glass, 87 μ corn pollen, and 46·5 μ copper) were measured in a grid-generated turbulence. The hollow glass beads were small and light enough to behave like fluid points; the other types had significant inertia and 'crossing trajectories' effects. The autocorrelations decreased much faster for heavier particles, in contradiction to previous experimental results. The integral scale for the copper beads was $\frac{1}{3}$ of that for the hollow glass beads. The particle velocity correlations and the Eulerian spatial correlation were coincident within experimental error when the separation was non-dimensionalized by the respective integral scale. The data generated by the hollow glass beads can be used to estimate Lagrangian fluid properities. The Lagrangian time integral scale is approximated by L/u', where L is the Eulerian integral scale and u' is the turbulence intensity.

1. Introduction

In order to predict the spread of aerosols and other foreign particulate matter by a turbulent flow, a knowledge is required of the statistics of the motion of small particles in response to the turbulent fluctuations of velocity. (A distinction is made here between a 'particle', a solid, rigid piece of matter immersed in the continuum, and a 'fluid point', a mathematical point moving with the continuum.) One could not hope to predict, nor would one want to predict, the position of each particle at every instant of time in a turbulent flow. What is desired are predictions of the quantities characteristic of the ensemble of particle paths from a distribution of properties of an ensemble of realizations of turbulent flows. As an example, consider the spreading of smoke from a smokestack in the atmosphere. One would like to be able to predict, from the Eulerian properties of the flow field, the concentration of smoke downwind of the stack.

So-called K-theories are commonly used to estimate dispersion. They postulate that the flux is proportioned to the gradient of concentration, in analogy with molecular diffusion. Since the diffusing mechanism is of the same scale as the property being diffused, the K-theories are fundamentally incorrect and have no real value in the physical sense (Tennekes & Lumley 1971).

A fundamentally correct theory of turbulent dispersion of fluid points is that of Taylor (1921), who initiated the theory 'diffusion by continuous movements'.

† Present address: Division of Meteorology, Environmental Protection Agency, Raleigh, North Carolina

The reason this theory has not been put to common use is that it is formulated in terms of Lagrangian rather than the much more easily measured Eulerian variables. Taylor's theory reduces the dispersion problem to that of determining the Lagrangian autocorrelation function. (Hereafter, the word 'Lagrangian' will be used in its strictest sense, to denote a set of co-ordinates in which each fluid point is fixed. A set of co-ordinates in which a foreign particle is fixed will be denoted by 'particle', e.g. particle velocity autocorrelation function.)

As originally stated, Taylor's theory applies only to a homogeneous flow and predicts the dispersion of fluid points rather than of foreign particles. The modification of the theory to make it applicable to particles is straightforward; the modifications required to make it applicable to non-homogeneous flows are not straightforward, but, in many cases, non-homogeneity may be taken into account (Monin & Yaglom 1965; Batchelor 1957).

A myriad of theories on dispersion of fluid points has been presented. Sutton (1947), for example, derived a practical set of expressions for the dispersion of fluid points in the atmosphere by making certain assumptions on the nature of the autocorrelation function. His equations contain constants which must be chosen empirically in accordance with certain gross features of the dispersing flow; they do not accurately predict the dispersion in most cases. It must be recognized that the dispersion of fluid points is a special case of the particle dispersion problem, and, as such, none of these theories accounts for the lack of coincidence between paths of particles and those of fluid points.

Tchen (1947), Lumley (1957), and others have attempted to predict dispersion from the dynamical equation describing the motion of particles. Lumley (1957) and Corrsin & Lumley (1956) have pointed out errors in the earlier analyses which make their results somewhat uncertain. Lumley concluded that the problem can be resolved only on the level of functional probabilities. In essence, he says that, in order to predict the probability of a particle travelling from one point to another, one must integrate, in function space, over all possible paths between two points, the probability of the particle taking the path. The theory of functions and function spaces is simply not yet developed to a point where such a calculation could be carried out, although elementary steps have been made (Lumley & Corrsin 1959; Lumley 1960; Patterson & Corrsin 1966).

Many experiments of the pure Lagrangian type have been performed. These experiments consisted of 'tagging' fluid points, either through a hot wire stretched across the flow field or through releasing a foreign gas, and measuring the distribution of tagged particles at intervals downstream from the source, the flow field being either the core of a fully developed pipe flow or the lee of an array of bars. Two uncertainties resulted from these experiments: (i) the effects of turbulent dispersion and molecular diffusion were not easily separated, and (ii) since tagged fluid points could not be followed individually, the autocorrelation functions, if obtained, were found through the questionable step of doubly-differentiating the second moment of the distributions.

Concerning the first problem, Taylor (1935) pointed out that molecular diffusion and turbulent dispersion are statistically independent, so that the variances due to these two effects are additive. Townsend (1954), and Batchelor

& Townsend (1956), however, showed that the two effects are synergistic. Later, Saffman (1960, 1961) pointed out a fallacy in their argument. He and Okubo (1967) have shown that the interaction *reduces* the dispersion relative to the origin from the value it would have had if the two processes had been independent and additive. (They also showed that the interaction *increases* the dispersion relative to the centroid of the diffusing patch.) Saffman claimed that his predictions were in qualitative agreement with the measurements of Mickelsen (1960), but both Saffman and Mickelsen suggested that further experimentation was needed to resolve this problem for large times. Concerning the second problem, graphical differentiation is always difficult, but the double-differentiation of an empirical curve, even one in which the scatter of the data is seemingly small, can give results which vary widely from one analyst to another. It appears that Kennedy's (1965) double-differentiation may have led him to incorrect conclusions about his results (see later comments).

Three laboratory investigations of the dispersion of particles deserve comment. Vanoni & Brooks (1955) injected neutrally buoyant fluid particles into the grid-generated turbulence of a water tunnel. They were the first to make measurements of successive displacements of particles and compute the 'Lagrangian' autocorrelation function directly from the decay-corrected velocity data. However, there are some problems with their data: (i) they reported difficulties with the injector strut inducing large disturbances into the flow, (ii) the sample size was very small (the largest number of trajectories in any one run was 34); (iii) turbulent intensities were not directly measured, but were inferred from the particle motion, and (iv) their data were partially but not completely decay-corrected.

Frenzen (1963) improved upon the work of Vanoni & Brooks, and extended the problem to include stably, unstably, and neutrally stratified flows. He photographed successive displacements of neutrally buoyant one millimetre droplets of nitrobenzene and olive oil in the grid-produced turbulence in a towing tank (water). He also encountered some problems: (i) the sample size was quite small (the largest number of trajectories was 50), (ii) turbulence intensities were inferred from particle motions, (iii) the mean flow and departures from homogeneous turbulence decay were found to be significant (he discussed these at length), and (iv) according to Shirazi, Chao & Jones (1967), he used an unusually high digital filtering which cut out perhaps as much as 50 % of the turbulent energy. (This is in rough agreement with the criteria developed for the sampling rate in § 3.)

Kennedy (1965) measured the dispersion of heat, 1250 μ soap bubbles, and 700 μ and 900 μ polystyrene beads in the grid-generated turbulence of a vertical wind tunnel. Comparisons with his data are difficult for several reasons: (i) his measured turbulence intensities were found to be abnormally low (see later discussion), (ii) his measured Eulerian spectral energy data were found to be inconsistent by Shirazi, Chao & Jones (1967), and (iii) his double-differentiation of the dispersion curves is questionable (see later discussion). Also, Kennedy did not measure particle velocities directly, but inferred them from the initial slope of the dispersion curve.

To the authors' knowledge, the three experiments described immediately above are the only ones in which the decay-corrected particle velocity autocorrelation function was computed from successive displacements of individual particles dispersing in a homogeneous, decaying field of turbulence.

Yudine (1959) discussed the physical behaviour of heavy particles with large terminal velocities. He stated that the process of dispersion depends upon the terminal velocity in three ways: (i) The terminal velocity determines the vertical displacement of the centre of dispersion of the particles. This effect is easily accounted for by introducing a convective term into the diffusion equation (Pasquill 1962). (ii) The terminal velocity is a measure of the inertia. Because of this, the particles do not completely follow the high frequency fluctuations of the turbulence. He claims this inertia effect is insignificant for diffusion times much larger than the particle time constant. (iii) If it has appreciable terminal velocity, a particle will fall from one eddy to another, whereas a fluid point would remain in the same eddy throughout the lifetime of the eddy. He has called this the 'crossing-trajectories effect'.

Csanady (1963) showed the inertia effect to be negligible but the crossing-trajectories effect and a consequential 'continuity effect' to be appreciable in the atmosphere. The 'continuity effect' arises in order to accommodate the 'back-flow' necessary to satisfy continuity. It results in correlations containing considerable negative loops, and, according to Csanady's estimates for the atmosphere, may reduce the effective lateral diffusivity by as much as a factor of four (as compared to the diffusion of a gaseous cloud). In an attempt to experimentally verify this estimate, Csanady (1964) found that the lateral diffusion was reduced, but that more careful experimental work was needed for a full appreciation of this effect. Csanady (1967) related the particle velocity correlation to the Eulerian spatial correlation taken along a vertical straight line representing the mean particle path. This analysis included the crossing-trajectories effect and ignored the particle inertia.

It is seen that very little is known about the particle velocity autocorrelation function, or, its limiting case, the Lagrangian autocorrelation function. No completely satisfactory theory exists nor have any completely satisfactory experimental data been generated. Previous experiments have failed to produce completely satisfactory data for numerous reasons, which were detailed previously. The specific goal of this work was to generate the data to allow conclusions to be drawn about the particle velocity autocorrelations. This involves (*a*) a range of particle parameters, but at least one particle type small and light enough to be considered a fluid point and one large and heavy enough to have significant inertia and crossing-trajectories effects, (*b*) following individual particle trajectories so as to avoid the questionable double-differentiation, (*c*) measurement of a sufficiently large number of particle trajectories to form statistically significant averages, (*d*) taking samples of particle velocities often enough so as not to ignore the small-scale motions, (*e*) having an observation time long enough to measure the full range of variation of the autocorrelation functions, (*f*) measurement of the Eulerian properties of the flow field, and, finally, (*g*) application of corrections to account for homogeneous decay of the turbulent flow field.

2. Theoretical considerations

Taylor's (1921) theory is well known. He showed that the mean-square fluid point displacement in a stationary homogeneous turbulence is given by

$$[Y^2(T)] = 2[v^2]\int_0^T \int_0^t \rho_{22}(t_1)\, dt_1\, dt, \tag{1}$$

where the square brackets denote ensemble averages,

$$\rho_{22}(t_1) = \frac{[v(t)\, v(t+t_1)]}{[v^2(t)]} \tag{2}$$

the autocorrelation function, and v is the fluctuating velocity following a fluid point. He also showed that

$$[Y^2(t)] = [v^2]t^2, \quad \text{for} \quad t \ll \tau_L$$

and

$$[Y^2(t)] = 2[v^2]\, T_L t, \quad \text{for} \quad t \gg T_L,$$

where τ_L is the Lagrangian Taylor microscale, and

$$T_L = \int_0^\infty \rho_{22}(t)\, dt \tag{3}$$

is the Lagrangian integral scale.

The equations are equally applicable for the dispersion of alien particles, provided that the velocities are interpreted as particle velocities, and that the Lagrangian time scales are interpreted accordingly. The problem with applying the Taylor equation is that the shape of the autocorrelation function (or, even the integral or microscales) is unknown.

Equation (1) can be doubly differentiated to obtain

$$\frac{1}{2}\frac{d^2}{dt^2}[Y^2] = [v^2]\rho_{22}(t). \tag{4}$$

This equation, then, was the basis for several previous experiments, as discussed in the introduction. The present experiment measures the autocorrelation function directly; i.e. by measuring particle velocities and taking lagged products, as in equation (2).

3. The design of the experiment

3.1. *Choice of flow*

Ideally, the starting point for the experiment would have been in a stationary and homogeneous turbulence. No such flow exists in nature, since homogeneous flows must be non-stationary, and stationary flows must be non-homogeneous. As indicated by previous experiments, the types of suitable flows are extremely limited.

A stationary grid flow was chosen because it is easy to construct, it has a flat mean velocity profile, and corrections can be made to account for the inhomogeneity. The tunnel was made the same size and speed as Kennedy's so that

direct comparisons could be made; i.e. 20 ft/sec air flow with a 1 in. grid, giving a grid Reynolds number of approximately 10 000. Since the decay corrections (see next section) could be made only in the initial period of decay, the test section was limited to 16 ft in length. A crude estimate indicated that 99 % of the particles would diffuse no more than 3 in. from the centreline, so that a 16 in. square test section was adequate.

The particle with the highest terminal velocity was the 46·5 μ copper bead, with an Oseen velocity of approximately 1·5 ft/sec. Since this particle was to spend about one second in the tunnel, during its trip through the test section, the particle would fall about 1·5 feet relative to the flow. Hence, it was necessary to place the test section vertically, with the flow upward. This had the slight additional advantage that the particle would spend a little more time in the initial period of decay.

3.2. *Analysis of decay*

During the initial period of decay the turbulence intensity changes by a factor of $\frac{5}{2}$ (Batchelor 1956), so that the turbulence in this region may not be regarded as homogeneous. This change, as seen by a fluid point, is rather slow, so that the grid flow is sometimes called a homogeneous, decaying turbulence, whereas it is obviously a non-homogeneous but stationary field. This effect is negligible for short time lags, although one might expect to see a difference between short lag correlations determined at various positions down the tunnel. For long lags, this effect is definitely important. Fortunately, there is evidence to suggest that during this phase of decay, the turbulence may be regarded as largely identical in structure with simple changes in length and velocity scales. An extension of these ideas to the particle and Lagrangian cases implies a simple change in time scale proportional to distance (or time) from the virtual origin of decay. With this co-ordinate stretching, the bias introduced by measuring the correlations in a mildly inhomogeneous turbulence, rather than a truly homogeneous one, can be removed. The following analysis was originally introduced by Taylor (1935) (from a somewhat different viewpoint), modified by Batchelor (1952), and shown to be sufficient to the task by Frenzen (1963). Batchelor used the concept in the analysis of diffusion in a decaying turbulence. Frenzen showed that measurements made in a homogeneous decaying field could be adjusted in such a way that data approximating the characteristics of a stationary one would result. It will be shown here that measurements made in a stationary, non-homogeneous field can be adjusted in such a way that data approximating the characteristics of a homogeneous one will result. (A transformation of $x = Ut$ makes this analysis identical to that of Frenzen.)

During the initial period, the turbulent energy follows the inverse linear decay law, $u'^2 \propto (x - x_0)^{-1}$, where x is the distance from the grid and x_0 is the location of the virtual origin of decay. In actuality, careful investigations have shown that this is not strictly true, but from a practical viewpoint, this law is sufficient; indeed, in order to make any correction at all, the assumption of an inverse linear law is a necessity. The prediction of this law requires the assumptions that the transfer and dissipative terms are equally important and that the spectra are self-preserving at all distances from the virtual origin (Lin 1961).

Also, any characteristic length scale of the turbulence (say L_E, the Eulerian integral length scale) increases as $(x-x_0)^{\frac{1}{2}}$. A time scale T^* characteristic of the decaying eddies can be defined from a velocity scale V^* and a length scale L^* of the turbulence. Hence,

$$T^* = \frac{L^*}{V^*} \propto \frac{(x-x_0)^{\frac{1}{2}}}{(x-x_0)^{-\frac{1}{2}}} = x-x_0, \quad \text{or} \quad T^* \propto x-x_0. \tag{5}$$

It thus becomes possible to apply suitable scale factors in such a way that the shifting but self-preserving spectral distributions characteristic of successively larger downstream distances are continuously corrected to a homogeneous state approximately representative of the uncorrected field at any arbitrary position. The position was chosen for convenience in this investigation to be $x/M = 73$; it is nearly half-way between the first two camera locations and was a position where turbulence measurements were made. The correction was made by: (i) Compensating for velocity decay by dividing observed velocity fluctuations by the root-mean-square fluctuation observed at that point. This is equivalent to Frenzen's multiplying by the square root of the time of observation. (ii) Compensating for increasing length scale by dividing separations used in the experiment by their central location.

As a consequence of (ii), a consecutive series of infinitesimal, normalized length intervals $d(x-x_0)/(x-x_0)$ becomes a new corrected length interval when integrated over a real distance in the experiment, i.e.

$$\xi = A \int_{x_1-x_0}^{x_2-x_0} \frac{d(x-x_0)}{x-x_0} = A \ln \frac{x_2-x_0}{x_1-x_0}. \tag{6}$$

The constant A can be adjusted so that ξ will match the length scale measured at $x/M = 73$. From the point of view of the particle, correlation separations should be measured in time rather than in space, so that, in actuality, the constant A was adjusted so that ξ would match the time scale measured at $x/M = 73$. With this new definition of ξ as a time scale, the normalized autocorrelation function becomes:

$$\rho_{22}(\xi) = \rho_{22}\left(A \ln \frac{t_2-t_0}{t_1-t_0}\right) = \frac{[v(t_2) \cdot v(t_1)]}{[v^2(t_2)]^{\frac{1}{2}} [v^2(t_1)]^{\frac{1}{2}}}. \tag{7}$$

$\rho_{22}(\xi)$ is the normalized autocorrelation of lateral particle velocities measured in a stationary, homogeneous turbulence field possessing characteristics of the grid-generated flow at $x/M = 73$.

3.3. *Particles*

There are two relevant parameters in this investigation. The first is the ratio of the particle time constant, given by $T_p = u_T/g$, to the smallest time scale of the motion, which is $t_K = (\nu/\epsilon)^{\frac{1}{2}}$. The second is the ratio of the particle diameter, D, to the smallest length scale of the motion, which is $\eta = (\nu^3/\epsilon)^{\frac{1}{4}}$, the Kolmogoroff microscale. The particle terminal velocity is u_T, g is acceleration due to gravity, ν is the kinematic viscosity, and ϵ is the rate of dissipation. Based on Kennedy's results, it was reasoned that particle parameters covering the range of two orders of magnitude below unity would provide all the information desired; i.e. that this

range would permit extrapolation to zero time constant, or, equivalently, that these particles would behave much like fluid points. All particles below $100\,\mu$ were less than a tenth of the smallest length scale, so that the time-scale ratio was expected to be the primary variable of interest. In order to investigate the effect of each of the particle parameters independently, two particles with the same time-scale ratio but different length-scale ratios and two with the same length-scale ratio, but different time-scale ratios were chosen. This required three particle types. A fourth particle, which had as small a time-scale ratio as was possible to work with, was added.

The particles used in this investigation were chosen on the basis of the above considerations and also on the basis of their availability, low cost, sphericity, uniformity of shape, ease of sieving, ease of injecting, and reflectivity. Table 1 lists the particles along with relevant parameters. It is to be noted that the definition of the particle time constant is not identical to that given by Lumley (1957). His definition is $T_p = D^2(1 + (2\rho_p/\rho))/36\nu$, which conforms to the definition $T_p = u_T/g$ if the particle obeys Stokes flow. As can be seen from table 1, only one particle had a Reynolds number less than one-half and hence obeyed Stokes flow. The definition used here is a better physical measure of the particle time constant, i.e. the time required for a particle subjected to a step change in velocity to reach 63 % of its final velocity. The terminal velocities were estimated by a method recommended by Fuchs (1964).

	Hollow glass	Solid glass	Corn	Copper
Diameter (μ)	46·5	87·0	87·0	46·5
Density (g/cc)	0·26	2·5	1·0	8·9
Time constant (msec)[a]	1·7	45·0	20·0	49·0
Time scale ratio[b]	0·145	3·85	1·72	4·21
Length scale ratio[c]	0·105	0·198	0·198	0·105
Stokes velocity (cm/sec)	1·67	56·2	22·5	57·0
Terminal velocity (cm/sec)[d]	1·67	44·2	19·8	48·3
Reynolds number	0·05	2·48	1·10	1·45

(*a*), based on terminal velocity; (*b*), the fluid time scale is 11·6 msec at $x/M = 73$; (*c*) the Kolomogoroff microscale is 0·043 cm at $x/M = 73$; (*d*) computed from table 5 in Fuchs (1964, p. 32).

TABLE 1. Particles and relevant parameters

It is to be noted from table 1 that the particle parameters are not two orders of magnitude below unity, as was desired. Based on Kennedy's (1965) estimates of the smallest turbulence time and length scales, the parameters would have been nearly two orders of magnitude below unity, but Kennedy's turbulence intensities and hence his dissipation were found to be abnormally small, making his smallest time and length scales abnormally large. The particle time constants used in this experiment are smaller than the solid particles used by Kennedy by a factor of three, and the time constant of the hollow glass beads is smaller than that of Kennedy's soap bubbles by a factor of six. The diameters are smaller by more than an order of magnitude.

Lumley & Snyder (1968) made a calculation showing that, for less than a 5 % error in the autocorrelation function, the small beads could vary by $\pm 9\,\mu$ and the large ones by $\pm 16\,\mu$. However, if the large particles varied by more than about 3 % in diameter, their terminal velocity would change enough so that they would no longer be within the field of view of the last camera. Of the several techniques tried for obtaining the narrow size range of particles, sieving was found to yield the best results. The guaranteed tolerance of the precision micromesh sieves was $\pm 2\,\mu$. The nominally $46{\cdot}5\,\mu$ beads were sieved through $45\,\mu$ and $48\,\mu$ sieves, so that theoretically the absolute range of particle sizes was $43\,\mu$ to $50\,\mu$. The $87\,\mu$ glass beads were sieved through $84\,\mu$ and $90\,\mu$ sieves. Sieving was found to be quite adequate, as evidenced by microscopic examination and by the fact that very few particles went out of the field of view of the last camera.

3.4. *Number of measurements required*

It is necessary to determine what number of particle trajectories is required for a specified accuracy in the measurement of the autocorrelation, or, said another way, to determine the likely error in the estimation of the autocorrelation from a non-infinite set of samples. If a number of independent measurements of the correlation of a Gaussian process are made, the mean-square relative error can be represented as $\epsilon_R^2 = (1 + 1/\rho^2)/N$, where ϵ_R is the relative error, ρ is the autocorrelation, and N is the number of measurements (Lumley & Panofsky 1964). Since the turbulence is very nearly Gaussian in many respects, this equation is very likely a reasonable estimate of the errors involved. For very small separations, the correlation is approximately unity, so that the number of runs required for less than 10 % error is about 200. For large separations, the correlation may be approximated by $\rho = e^{-t/T_L}$, and for separations of the order of the integral time scale, 700 measurements are required for 10 % accuracy. This accuracy is that relative to the value being measured; at large separations, this represents a very small percentage of the value at zero separation. For a 1 % error, 70000 measurements would be required, which is clearly beyond reason. Hence, it was decided to take 700 measurements at each separation and accept a possible 10 % error in the determination of the autocorrelation at large separations. These figures are in very close agreement with the experimental findings of Kennedy (1965), who made between 150 and 700 measurements, depending upon separation, to obtain stable averages.

3.5. *Sampling rate and observation time*

It is necessary to determine how frequently particle photographs need to be taken. If taken too infrequently, the mean particle velocity between frames will bear no relation to the velocity at the centre of the interval. If taken too frequently, unnecessary time and expense are incurred. The optimum sampling rate is hereby determined.

Moving with the mean velocity in a turbulent flow, there is negligible energy at frequencies above roughly $\frac{1}{2}(\epsilon/\nu)^{\frac{1}{2}}$. This is a consequence of Kolmogoroff's theories applied to the Eulerian time spectrum (Corrsin 1963*a*, Inoue 1951). In essence, dimensional analysis shows that $S(\omega) = \alpha\epsilon\omega^{-2}$ in the inertial subrange,

where S is the one-dimensional energy spectrum function (temporal), ϵ is the dissipation, ω is the frequency, and α is a universal constant. The peak of the dissipation spectrum occurs at $\kappa/\kappa_0 \sim \frac{1}{2}$, where κ is the wave-number, and κ_0 is the Kolmogoroff wave-number. In the absence of other information, it is perhaps not unreasonable to suppose that the cut-off in the second moment of the time spectrum will occur somewhere near $\omega/\omega_0 \sim \frac{1}{2}$, where ω_0 is the Kolmogoroff frequency, $\omega_0 = (\epsilon/\nu)^{\frac{1}{2}}$. On the basis of Kolmogoroff scaling, there is no reason to expect a difference between the Eulerian and Lagrangian time spectra. The Kolmogoroff frequency is therefore the Nyquist frequency. If a particle followed the turbulence perfectly, sampling at this rate would give all necessary information about the motion. In Kennedy's flow, this was $2000/((x/M)-10)$ Hz. Sampling at this rate, the number of measuring stations required between x_1/M and x_2/M is roughly

$$N_S = \int_{x_1/M}^{x_2/M} \frac{fM}{U} d\left(\frac{x}{M}\right) = 8{\cdot}5 \ln \left(\frac{\frac{x_2}{M} - 10}{\frac{x_1}{M} - 10} \right). \tag{8}$$

Since measurements were begun at 60 mesh length and stopped at 180 (the initial period of decay), this required 10 samples, taken progressively farther apart. It should be noted that this method of sampling corresponds to sampling at equal separations of the corrected time scale, defined by equation (6) or (7), provided the virtual origin of the particle energy is the same as that of the turbulence. Since this was found to be the case, the effective number of runs for short lag correlations was greatly increased.

Again, Kennedy's (1965) dissipation was found to be abnormally small, so that this estimate of the sampling rate was somewhat smaller than desirable. Fortunately, the particle velocity correlations were not strongly affected by this and some compensation was possible.

Roughly speaking, the maximum lag of interest is the Lagrangian time integral scale. A crude estimate for this time scale is $T_L = L_E/u'$, where L_E is the Eulerian spatial integral scale (roughly the mesh size) and u' is the root-mean-square fluctuating velocity. During this time, the particle will travel a distance UL_E/u', and at the turbulence level 200 mesh lengths downstream from the grid, this gives approximately 160 mesh lengths. Thus, observations can be made for times about the order of the Lagrangian time integral scale. This is a conservative estimate because the turbulence level is always higher than it is at $x/M = 200$.

3.6. *Photographic system*

It was desired to follow the trajectories of individual particles in order to avoid double differentiation of the dispersion curves. Since Kennedy's (1965) scheme was incapable of detecting particles smaller than about $700\,\mu$, ten individual still cameras spaced along the tunnel were used to photograph the particles. Since the flow was isotropic in planes perpendicular to the mean flow in Eulerian variables, it was isotropic in particle variables, e.g. particle position distributions in cross sections perpendicular to the stream were expected to be circular.

Perpendicular displacements were expected to be uncorrelated with each other and to have equal variances, so that all information could be obtained from measurements of a single component. Therefore, only the lateral particle displacements from fiducial marks were measured.

To minimize parallax errors and obtain a large depth of field, a large object distance was required. From the standpoint of lighting, a small object distance was required. Thus, there was an obvious conflict in requirements, and a compromise had to be made.

From geometrical considerations, it is easy to show that the worst case would result in an 18 % error in the measurement of the particle position with the optical system used. However, on the average, the parallax error is quite small; the contribution to parallax error from particles in front of the focal plane is nearly balanced by that from those behind the focal plane. Also, since it is not the absolute particle displacement, but rather the change in particle displacement ($\Delta y/\Delta t$) which is of most interest, the parallax error is a second-order effect.

Snyder (1969) showed that for the chosen object distance of 50 in., the error due to parallax in estimating the autocorrelation of particle velocities was less than 0·12 %, i.e.

$$\frac{[v'(t)\,v'(t')]-[v(t)\,v(t')]}{[v(t)\,v(t')]} \leqslant 0{\cdot}0012,$$

where $[v'(t)\,v'(t')]$ is the apparent autocorrelation, and $[v(t)\,v(t')]$ is the true autocorrelation.

4. Apparatus and instrumentation

4.1. *The wind tunnel*

The wind tunnel shown in figure 1 was designed and built specifically for use in this investigation. Entering air was cleaned with filters which removed 99·97 % of 0·3 μ particles to prevent spurious particles of dust from spoiling the photographs. The rating of the blower was 2200 cfm at $4\frac{1}{2}$ in. static pressure. The right-angle bend and wide-angle diffuser were necessitated by a limited vertical space. The plenum chamber and contraction served to dampen the turbulence and provide a flat mean velocity profile in the test section. The test section was nominally 16 in. × 16 in. × 16 ft. Three of the walls were slightly divergent and the fourth wall was adjustable; this was done so that the core flow could be made independent of downstream distance regardless of the boundary-layer growth. Two opposite walls contained 8 in. wide glass windows. A third wall was removable; it could be fitted with probe mounts for flow measurements or with light sources for illumination. A 5 in. section of honeycomb ($\frac{3}{16}$ in. hexagonal cells) at the exit of the test section prevented the flow from prematurely diverging.

The biplane grid was made from $\frac{3}{16}$ in. square brass rods spaced on 1 in. centres; its solidity was 0·34. It contained a slot to house the particle injection tube and electrical leads to the photocell.

The test section was braced to a vertical wall for support and alignment. The mean flow speed was set at 6·5 metres per second (21·5 feet per second). The room temperature was maintained at approximately 26° C and the humidity at

approximately 40 % throughout all measurements. The humidity control was necessary because the terminal velocity of the corn pollen was dependent on the humidity.

4.2. *Optical and illumination systems*

It was originally felt that a large magnification was required, something like 1 : 1. Using the same criteria as Welford (1962) for the acceptable blur of an out-of-focus image, it was calculated that the aperture should be something like $f/500$, which is clearly ridiculous in terms of available lenses and the tremendous amount of light required. When smaller magnifications were tried, success was achieved.

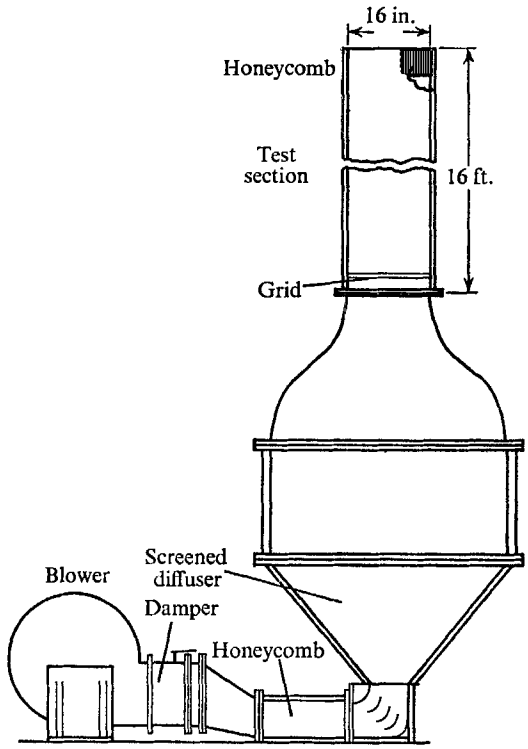

FIGURE 1. The wind tunnel.

If all that is desired is the particle position (not resolving the shape of the particle), then the demagnification is immaterial, except as it affects resolution; that is, the spot size remains constant while the field size is reduced. The accuracy with which the particle may be located is progressively reduced. This accuracy is, in any event, much greater than the accuracy of other elements in the system.

With the small magnifications, it was possible to use 35 mm film. The camera bodies were Robot Star II/50, which contained spring motors for taking 50 one-inch square frames before being rewound. The cameras contained solenoids for remote shutter control. The lenses were Schneider 'Componon' with focal lengths of 105 mm and largest apertures of $f/5{\cdot}6$. The system demagnification was approximately 11 : 1.

The film used was 35 mm, 2479 RAR, a Kodak instrumentation film with an ASA speed of 400. Faster films were available, but they were much more grainy (the granularity is important when considering the accuracy with which the centre of the particle image may be located).

The optical and lighting arrangement is shown in figure 2. The light source was placed far from the field of view so that the windows were not directly illuminated. Thus, foreign matter on the windows lessened the amount of light reflected by the particles onto the film, but did not obscure the particle images. The xenon flash-tubes were 3 in. in length, type FX-38A-3, from E.G. & G., Inc. The energy storage was 200 J and the flash duration was about 300 μs. The characteristic fast

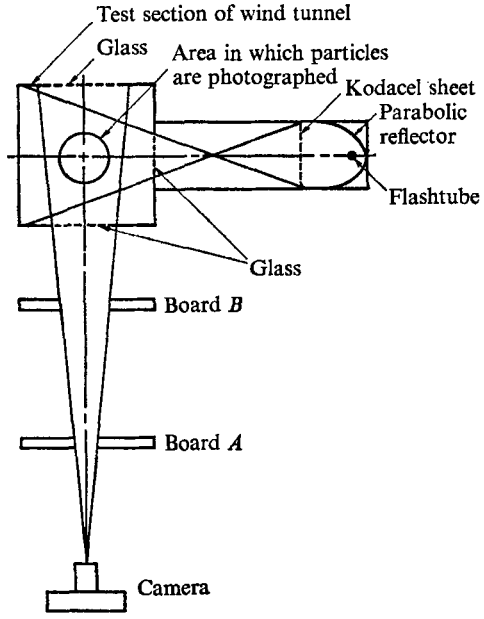

FIGURE 2. Optical and illumination systems.

rise and slow decay of the light output from the flashtubes proved to be extremely advantageous; as a result of this, images of moving particles were easy to detect amid the background noise because of their characteristic comet shape. Stationary particles such as dust on the windows were round in addition to being out of focus. Also, imperfections in the film emulsion were not, generally speaking, of comet shape.

Sharp and clear fiducial marks from which to measure particle positions were reflected through mirrors into the cameras. In figure 2, board *A* contained the fiducial marks, and board *B* held the mirrors. Counter numbers, identifying the camera, the particle type, and the trajectory were reflected into the cameras in the same manner.

4.3. *Film reading*

The particle positions (distances from fiducial marks) were measured by Glenn Engineering Services, Inc., on a Benson Lehner Oscillograph Analyzer and Reader (OSCAR). The OSCAR is able to resolve the field into about 6000 parts

(in each direction), so that, providing the centre of the particle image can be located precisely, the absolute accuracy is about 0·001 in. (the field size was 8 in.). An independent set of measurements showed that the root-mean-square deviation from the mean was 0·0034 in. Snyder (1969) showed that this error was insignificant in calculating the autocorrelations (less than 0·35 %).

To calibrate the system, a thread was strung along the centreline of the wind tunnel and the thread and a scale were photographed against the background of the fiducial marks at each camera station. Appropriate measurements were made to enable conversion from OSCAR units to physical dimensions in the wind tunnel.

In order to account for changes in magnification in any of the cameras or in the OSCAR, the distance between the two fiducial marks was measured on the first frame of each filmstrip. This was the filmstrip calibration, since the distance between fiducial marks and the centreline of the wind tunnel had previously been determined. After calibration, the distance between the particle and one fiducial mark was measured for each frame of the strip, camera and trajectory numbers being recorded simultaneously.

Occasionally, and for various reasons, a particle image could not be found on the film in one of the ten cameras. If the particle was missing in the first or last camera, or in more than one camera, the entire trajectory was discarded. If otherwise, the missing particle position was replaced by the arithmetic mean of its positions in the two adjacent cameras. Snyder (1969) made a full analysis of the influence of this replacement on the statistics. In general, the error in determining the mean-square particle velocity was much less than 1 %; the worst case resulted in a 4·7 % error. The relative error in determining the autocorrelation for moderate and large separations was less than 4 %, which is less than the accuracy obtainable because of the finite number of particles. The absolute error goes to zero for large separations.

4.4. *Particle injector and detector*

The particle injector used for the corn pollen, solid glass beads, and copper beads is shown in figure 3. Filtered dry air was fed to the system through a pressure regulator and flowed through a fine-mesh screen (to contain the beads) into a narrow angle expansion, from which it exited to the room through paper filters. Particles were introduced into the expansion and the flow rate was adjusted so that the beads were kept in suspension. They were then entrained by the air flow through the sampling tube in the side of the expansion and carried to the centre of the tunnel. Valves A and B were adjusted simultaneously to maintain the beads in suspension and to control the pressure inside the expansion (hence to control the air flow rate in the sampling tube). The particle concentration was adjusted to maintain a particle flow rate through the sampling tube of about one bead per second. In order to keep the beads in suspension, it was necessary to vibrate the injector; hence, the concentration was controlled mainly by the rate of vibration.

This injector worked quite well for the heavier particles, which left the walls of the diffuser as single beads. The hollow glass beads, being much smaller and

lighter, had a much greater tendency to agglomerate. A similar type injector was constructed for these; here, the $46\frac{1}{2}\mu$ hollow glass beads were placed in a 48μ micro-mesh sieve, so that they had to pass through the sieve as singles before being entrained by the air flow entering the sampling tube.

The sampling tube was run through the centre bar of the grid to the centre of the tunnel; it was not seen by the flow. There, it made a rather sharp 90° bend and continued downstream twenty inches through a $\frac{3}{16}$ in. diameter tube which also housed the leads to a photocell. The particles were ejected at the wind tunnel centreline 20 mesh lengths from the grid with a mean velocity the same as the tunnel speed. Hot-wire probes were unable to detect any effect from the sampling tube on the mean velocity or the turbulence intensity beyond $x/M = 41$ (the first camera was stationed at $x/M = 68$).

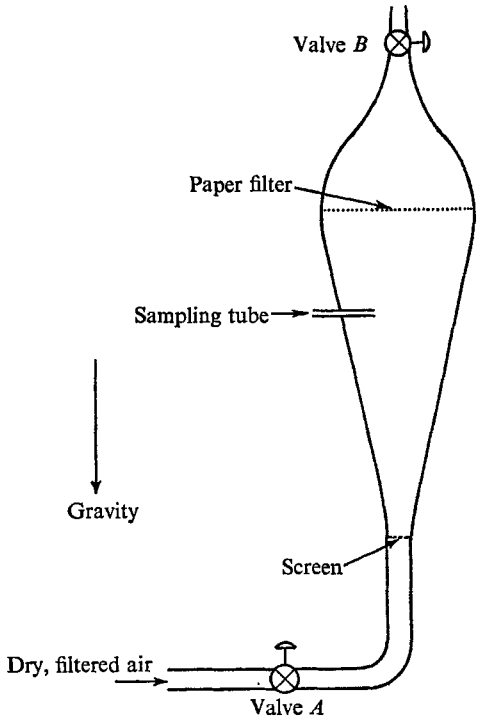

FIGURE 3. Heavy particle injector.

Since the time of entrance of the particles into the tunnel was random, a detector was required. This consisted of a laser beam directed across the end of the sampling tube and a tiny photocell; the particles exiting from the sampling tube crossed the laser beam and reflected light into the photocell, which produced an electrical pulse at the instant the particle entered the tunnel. The photocell was a Hoffman EA7-E1 ($\frac{1}{16}$ in. diameter).

A 4 mW, helium–neon laser was necessary for detecting the smallest beads; a 1 mW one was sufficient for the larger beads. An amplifier with a gain of 10 000 was constructed from Philbrick operational amplifiers to match the photocell with the timing system.

4.5. *Timing system*

A typical run (i.e. taking 10 pictures of one particle as it travelled through the test section of the tunnel) proceeded as follows. All lights in the enclosure were off. A particle entered the tunnel and triggered the timing system. The timing system indexed a set of counters (frame identification numbers) by one count, opened the camera shutters (all ten at once), turned on the lights illuminating fiducial marks and counter numbers, triggered the ten flashes in sequence as the particle entered the field of view of the respective camera, and, after the tenth flash fired, closed the camera shutters.

Because all ten pictures of a particle had to be taken within $\frac{1}{2}$ sec, because a large number of trajectories were involved, and because it had to perform several varied tasks, the timing system had to be accurate, reliable, and versatile. For these reasons, a digital system consisting of plug-in microcircuits (μ-PACS) from Honeywell, Inc. was used. The timing system utilized a crystal oscillator clock, binary counters, NAND gates, and lamp drivers to trigger the flash tubes, control the camera shutters, and index the counters. The accuracy of the timing of the flashes was better than $\pm$ 1 msec ($\frac{1}{4}$ in. of particle travel).

4.6. *Other equipment*

All of the Eulerian turbulence data measured in this work were obtained with a constant-temperature hot-wire anemometer designed by Wyngaard & Lumley (1967). This particular anemometer was designed for a flat response to 2 kHz, which corresponds to $\kappa\eta = 0{\cdot}8$ at $x/M = 66$, where κ is the wave-number and η is the Kolmogoroff microscale. Hence, the output contained all the significant high frequency information about the flow. The hot wire was tungsten, flash-plated with platinum, had a diameter of 0·0003 cm, a length of 0·06 cm, and was operated at an overheat ratio of 0·8. l_w/d was 200 and l_w/η was 1·5 at $x/M = 66$, where l_w is the wire length and d is the wire diameter. The length to diameter ratio was somewhat less than desirable (Champagne *et al.* 1967). Since the only way to increase this ratio without limiting the spatial resolution was by lowering d, and since smaller diameter wires are exceedingly difficult to work with, it was decided to accept this ratio and make the corrections suggested by Champagne *et al.* Concerning the spatial resolution, Wyngaard (1968) has shown that the measured spectrum does not deviate significantly from the true spectrum for $\kappa l_w < 1$, provided $l_w/\eta < 3$. In this flow, it was unnecessary to take measurements at frequencies corresponding to values of κl_w larger than one, so that it may be assumed the measured spectra do not deviate significantly from the true spectra.

An adder–subtracter circuit was constructed from Philbrick solid state operational amplifiers for use with the two channel anemometer (x-array). It had a flat response to 5 kHz.

Spectral analysis was done with a Hewlett Packard 302 A wave analyzer. Turbulent signals were squared with a Ballentine 320A voltmeter. All averages were obtained from an integrator using a Philbrick SP 656 chopper-stabilized operational amplifier. Half-minute integration times were generally found to be sufficient. A Hewlett Packard 3440 A digital voltmeter was used to read d.c. voltages.

5. Presentation and discussion of results

5.1. *Eulerian turbulence data*

The flow measurements in this work were made for two reasons: first, to 'proof' the tunnel so that particle dispersion measurements could be started, and second, to describe the necessary characteristics of the turbulence in order to provide a basis of comparison with the characteristics of the particle motion.

Mean velocities were measured with a Pitot tube and Meriam micromanometer, accurate to 0·001 in. of water. The mean velocity profiles were flat, varying less than 1 % over the core (approximately an 8 in. square area). The wall was adjusted so that the mean velocity in the core was the same at all distances from the grid.

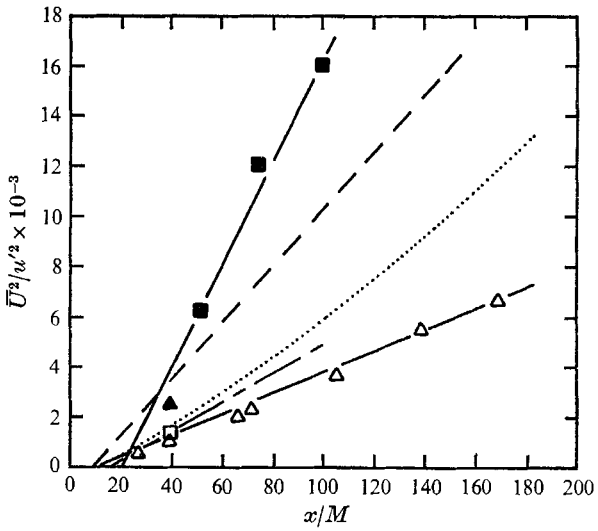

FIGURE 4. Comparison of turbulent energy decay. ■, Kennedy; – – –, Batchelor & Townsend (round bars); △, present data; ▲, Corrsin (round bars); ——, Baines & Peterson (σ = 0·44); □, Corrsin; ·····, Comte-Bellot & Corrsin. All data for square bars and σ = 0·34, unless otherwise noted.

The following measurements were made with a single hot wire, stretched perpendicularly to the mean flow.

The turbulence was found to be homogeneous in planes parallel to the grid. Even close to the grid, the intensity profiles were nearly flat, varying by about 10 % over a 9 in. core. This small variation was undoubtedly due to the amplifying effect of the turbulence on the small imperfections or inhomogeneities in the grid and is in reasonable agreement with measurements made by Grant & Nisbet (1957). The profiles were more nearly flat with increasing streamwise distance, but the size of the core decreased because of the growing turbulent boundary layer. Even at the farthest downstream distance, however, the core size was well over 7 in., which was adequate for the particle measurements.

The following group of measurements was made with cross-wire probes. The measurements of the decay of the turbulent energy in the streamwise direction are compared with the results of other investigators in figure 4. The data of

Batchelor & Townsend (1948) are for a square mesh, round bar grid; it is well known that square bar grids generate a higher turbulence intensity than do round bar grids of the same solidity (Corrsin 1963*b*). The present data can thus be expected to be lower than the data of Batchelor & Townsend, since it is the inverse of the turbulent energy which is being compared. The data of Baines & Peterson (1951) were for a higher solidity mesh, but compare favourably with the present measurements. Corrsin's (1963*b*) result for the round bar grid is, as expected, higher than the present data, and his result for the square bar grid compares favourably with the present data. Comte-Bellot & Corrsin's (1966) data compare reasonably well. The only data that do not compare favourably are Kennedy's (1965), whose external flow conditions are nearly identical to those of the present experiment.

It was originally intended to match the flow conditions of Kennedy, but in view of the above discussion, this intention was discarded, and measurements of particle dispersion in a more 'standard' flow were made. The discrepancy is unfortunate because the present experiment was designed using Kennedy's data to estimate particle to fluid length- and time-scale ratios and the sampling rate. Since Kennedy's turbulent energy was much smaller than that measured here, the estimated dissipation was too small; hence, the estimated sampling rate was too small, the estimated fluid length scales were too large, and the estimated fluid time scales were too large. Some compensation for the low sampling rate was possible and will be discussed later. However, it was hoped to have one particle type which would follow the flow perfectly, and hence to obtain pure Lagrangian data. In the present flow, this was found impossible.

Figure 5 shows the energy decay curves (along centreline of test section). As mentioned previously, corrections were made to account for the finite wire length, as suggested by Champagne & Sleicher (1967). They showed that, for the particular wires used here $\overline{v^2}_{\text{true}} = 1{\cdot}17\overline{v^2}_{\text{measured}}$, and this correction was used throughout. As shown in the figure, the energy of the longitudinal velocity component is nearly equal to that of the lateral component, indicating that the flow is nearly isotropic. Because of the disagreement with the Kennedy's data, a Thermo-Systems constant-temperature anemometer and a single wire perpendicular to the flow were used at this point as a check on the present data. The data obtained in this manner agree excellently with the cross-wire data and are also plotted in figure 5. The energy decay curves are adequately represented by

$$\frac{\overline{U}^2}{\overline{u^2}} = 42{\cdot}4\left(\frac{x}{M} - 16\right), \tag{9}$$

and

$$\frac{\overline{U}^2}{\overline{v^2}} = 39{\cdot}4\left(\frac{x}{M} - 12\right). \tag{10}$$

The normalization of the spectra was accomplished through the following convention:

$$\overline{v^2} = \int_0^\infty F_2(\kappa)\, d\kappa, \tag{11}$$

where F_2 is the energy spectrum function of the lateral velocity component. The spectral data were checked by comparing the dissipation calculated from the

spectra with that calculated from the energy decay relationship. For isotropic turbulence, this relation is

$$\epsilon = -\frac{\overline{U}}{2}\frac{d\overline{q^2}}{dx} = 15\nu\int_0^\infty \kappa^2 F_1(\kappa)\,d\kappa, \tag{12}$$

where $U(d/dx)$ has been substituted for d/dt, $\overline{q^2} = \overline{u^2}+\overline{v^2}+\overline{w^2}$, ϵ is the dissipation, ν is the kinematic viscosity, and F_1 is the energy spectrum function of the streamwise component. w^2 was taken equal to v^2. Measurements not presented here showed this to be the case. Reasonably good agreement was found between the

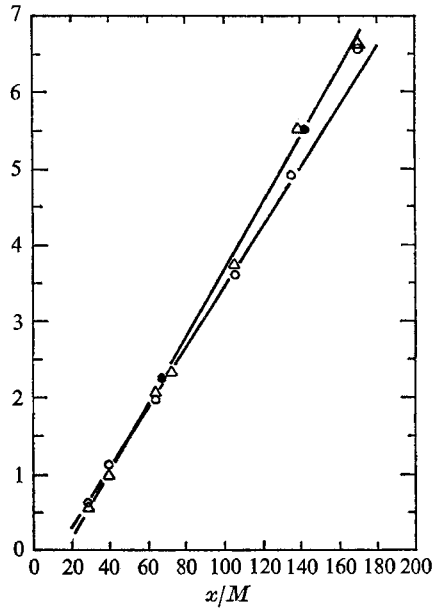

FIGURE 5. Decay of turbulent energy, ▲, $U^2/\overline{u^2}\times 10^{-3}$; ○, $\overline{U^2}/\overline{v^2}\times 10^{-3}$; ●, single wire check with Thermo-Systems anemometer.

dissipations calculated via the two methods. For example, at $x/M = 171$, the dissipation calculated from the spectra was 170 cm^2/sec^3; from the energy decay, it was 165 cm^2/sec^3. The spectral energy data are plotted in Kolmogoroff co-ordinates in figure 6, where $F_0 = (\epsilon\nu^5)^{\frac{1}{4}}$, $\kappa = 2\pi f/U$, and $\eta = (\nu^3/\epsilon)^{\frac{1}{4}}$, where ϵ was calculated using (10).

As expected, all of the spectra collapse (with the understandable exception at $x/M = 41$), when plotted in Kolmogoroff co-ordinates. This shows that the energy spectra are self-preserving, which is one prerequisite for applying the decay corrections. The second prerequisite, that the energy be inversely proportional to the distance from the virtual origin, is shown to be satisfied in figure 5. The third prerequisite, that the characteristic length scale be proportional to the square root of the distance from the virtual origin, is a consequence of the first prerequisite, the assumption of isotropy, and the definition of λ, the Taylor microscale, as the characteristic length scale,

$$\frac{1}{\lambda^2} = -\left(\frac{\partial^2 f(r)}{\partial r^2}\right)_{r=0}, \tag{13}$$

where f is the longitudinal correlation function, and r is the separation. von Kármán & Howarth (1938) have shown that, for the decay of turbulence behind a grid, this assumption and definition lead to

$$U\overline{du^2}/dx = -10\nu\overline{u^2}/\lambda^2. \tag{14}$$

Since $\overline{u^2} = A(x-x_0)^{-1}$, then

$$\lambda^2 = (10\nu/U)(x-x_0). \tag{15}$$

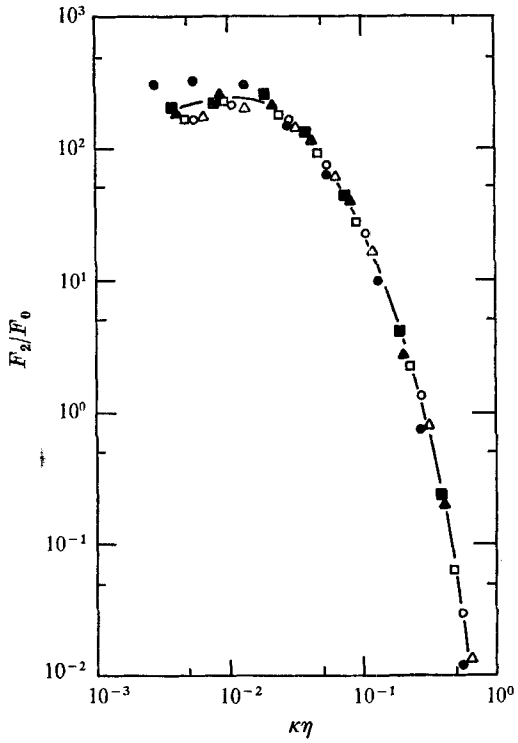

FIGURE 6. Lateral energy spectra. $x/M =$: ●, 41; ■, 66; ▲, 73; □, 106; ○, 138; △, 171.

Table 2 lists various flow parameters. The Taylor microscale was computed from (15). The integral scales were computed from

$$L_u = \frac{\pi}{2\overline{u^2}} F_1(0). \tag{16}$$

The dissipation was calculated using (9), (10) and (12).

A typical lateral Eulerian spatial correlation, $g(r)$, is shown in figure 7. This correlation was obtained by numerically integrating the equation

$$\overline{v^2}g(r) = r_{22}(r,0,0) = \int_0^\infty F_2(\kappa)\cos\kappa r\, d\kappa, \tag{17}$$

where $r_{22}(r,0,0)$ is the lateral spatial velocity correlation with separation in the streamwise direction.

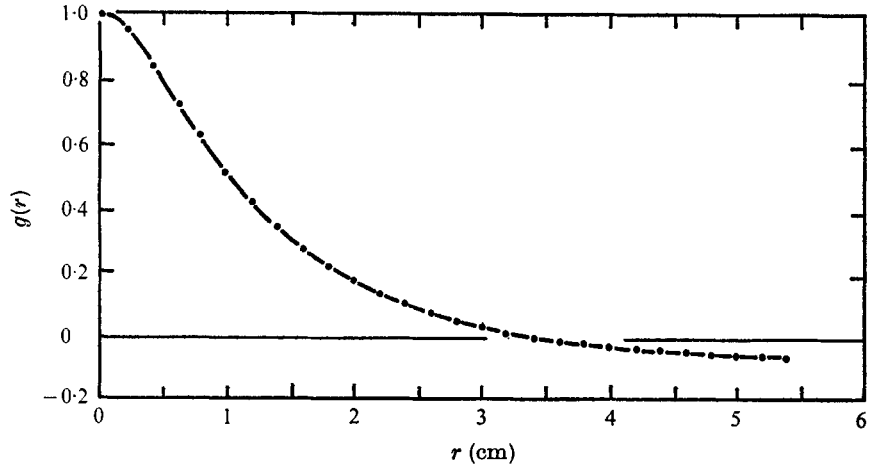

FIGURE 7. Eulerian lateral spatial correlation at $x/M = 73$.

x/M	41	64	73	107	138	171
u'/U (%)†	3·1	2·2	2·0	1·6	1·4	1·2
v'/U (%)	3·0	2·2	2·0	1·6	1·4	1·3
ϵ (cm²/sec³)	5430	1610	1160	480	266	165
η (cm)	0·029	0·039	0·043	0·053	0·061	0·069
λ (cm)	0·39	0·54	0·59	0·74	0·86	0·97
t_K (msec)	5·3	9·8	11·6	18·0	24·2	30·6
L_u (cm)	2·8	3·0	3·1	3·7	4·2	4·6

† $U = 6{\cdot}55$ m/sec.

TABLE 2. Eulerian turbulence data

5.2. *Particle data*

Particle pictures were taken at ten stations, spaced logarithmically (from the virtual origin of decay) from $x/M = 68{\cdot}4$ to 168.

Data analysis. The particle positions were recorded directly on IBM cards by the OSCAR. Appropriate data manipulations were done on an IBM 360/67 computer.

It was indubitable that the OSCAR operator would occasionally measure a spot on the film which was not a particle image. In order to guard against this, it was necessary to test each trajectory for flukes. This was done by testing to see if the difference between particle displacements in two adjacent cameras was within a specified discrimination level. If not, the trajectory was discarded. The question of what discrimination level should be used was critical. One would like to find a wide range of discrimination levels over which the total number of trajectories accepted would be unchanged. This was found to be nearly the case for the corn pollen data, the first to be analyzed. The lowest discrimination level, then, was the one used for the remaining data. For the hollow glass beads, however, it was necessary to increase the level slightly because its dispersion was much greater.

The discrimination levels, the total number of particle trajectories used in the calculation of the statistics of the particle motion, and the likely relative error in determining the correlations when the true correlation has a value of 0·1 are shown in table 3 for each particle type.

Particle type	Disc. level (in.)	Number of trajectories	Error (%)
Corn pollen	0·60	846	11·9
Glass beads	0·60	736	13·7
Copper beads	0·60	659	15·3
Hollow glass beads	0·65	651	15·5

TABLE 3. Discrimination level, number of trajectories, and likely relative error in autocorrelation

As this work was originally conceived, a Fourier series was to be fitted to each of the particle trajectories and each series was to be differentiated to obtain particle velocities. The behaviour of Fourier series is ideal in the sense that the derivative series contains no higher frequencies than does the original series. Hence, the conventional high frequency noise introduced by differentiation is not present with this type of curve fit. However, all attempts to fit Fourier series to this data resulted in failure. The reason is because the sampling rate was somewhat lower than desirable; aliasing (Lumley & Panofsky 1964) resulted because the highest frequency particle motions were not contained in the data. However, aliasing affects the spectrum only; it does not affect the autocorrelation.

The only recourse was to calculate particle velocities as the quotient of displacement divided by time between cameras. The velocity determined in this manner is, of course, the average velocity between the two cameras, so that this method results in some smoothing which reduces the root-mean-square velocity. The autocorrelation computed in this manner represents the true value at the points $t_1, t_2, \ldots, t_n$, of the autocorrelation of the smoothed signal.

$$\tilde{v} = \frac{1}{\Delta}\int_{-\frac{1}{2}\Delta}^{\frac{1}{2}\Delta} v(t+\xi)\,d\xi = \frac{y(t+\frac{1}{2}\Delta)-y(t-\frac{1}{2}\Delta)}{\Delta}, \tag{18}$$

where the tilde indicates smoothing, v is the particle velocity, y is its displacement, and Δ denotes the time separation between cameras (ignoring the fact that the intervals are not the same and that the velocity is not stationary).

Evidently, some of the high frequency content of the signal was removed. It was replaced in the following manner. The Fourier transform of the smoothed signal is

$$\hat{\tilde{v}}(\omega) = \tilde{v}(\omega)\frac{\sin(\frac{1}{2}\omega\Delta)}{\frac{1}{2}\omega\Delta}, \tag{19}$$

where the hat signifies the transform and ω is the frequency measured in radians per second. The spectral transfer (filter) function is given by

$$\psi(\tfrac{1}{2}\omega\Delta) = \frac{\sin^2(\frac{1}{2}\omega\Delta)}{(\frac{1}{2}\omega\Delta)^2}, \tag{20}$$

which is plotted in figure 8. In the figure, f is measured in Hz. Ideally, the filter function would be unity from zero to the Nyquist frequency, then drop to zero very rapidly thereafter. The filter function used here yields the exact value at isolated points of the true autocorrelation of the smoothed velocities, i.e. the velocities seen through this filter. It is impossible to regain any information beyond 1, and probably not much beyond $\frac{1}{2}$; on the other hand, the values below $\frac{1}{2}$ may be substantially improved.

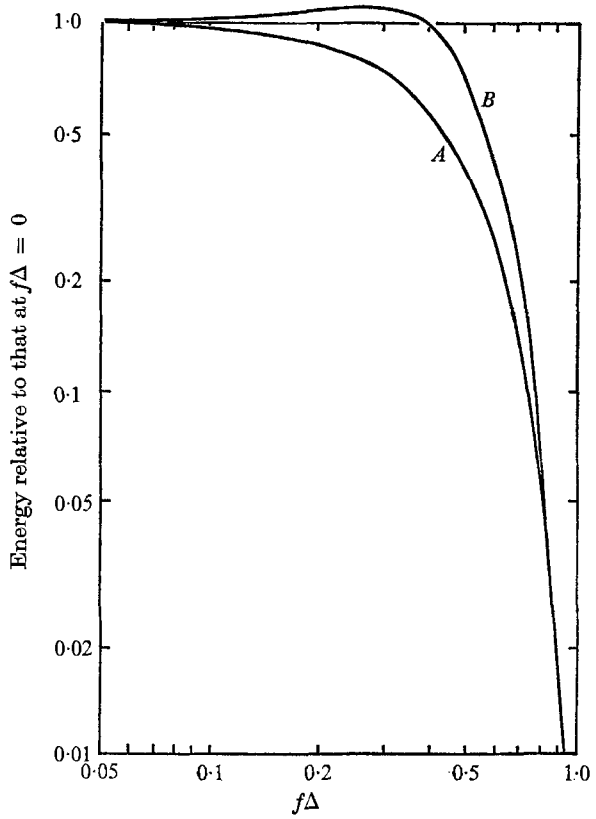

FIGURE 8. Filter functions. A, no compensation; B, slight over-compensation.

The smoothed second derivative of the true velocity is defined as follows

$$\tilde{v}''(t)\Delta^2 \equiv (\tilde{v}'(t+\tfrac{1}{2}\Delta)-\tilde{v}'(t-\tfrac{1}{2}\Delta))\Delta = \tilde{v}(t+\Delta)-2\tilde{v}(t)+\tilde{v}(t-\Delta). \tag{21}$$

The smoothed first derivative may be written as

$$\tilde{v}'(t+\tfrac{1}{2}\Delta)\Delta = \tilde{v}(t+\Delta)-\tilde{v}(t) = \int_t^{t+\Delta} \frac{\partial \tilde{v}(\eta)}{\partial \eta}\, d\eta. \tag{22}$$

Making the substitution $\eta = t+\xi+\frac{1}{2}\Delta$, this equation becomes

$$\Delta\tilde{v}'(t+\tfrac{1}{2}\Delta) = \int_{-\frac{1}{2}\Delta}^{\frac{1}{2}\Delta} \frac{\partial \tilde{v}(t+\xi+\frac{1}{2}\Delta)}{\partial \xi}\, d\xi. \tag{23}$$

With these definitions, it is not difficult to show that

$$\tilde{v}''(t)\Delta^2 = \int\int\int_{-\frac{1}{2}\Delta}^{\frac{1}{2}\Delta} v''(t+\xi+\zeta+\eta)\,d\eta\,d\zeta\,d\xi. \tag{24}$$

Notice that equation (24) is not an approximation, but an exact formula. $\tilde{v}''(t)\Delta^2$ is merely a convenient notation for the second differences in particle displacements.

The Fourier transform of (24) is

$$\hat{\tilde{v}}''(\omega) = -4\left(\frac{\sin\frac{1}{2}\omega\Delta}{\frac{1}{2}\omega\Delta}\right)\tilde{v}(\omega)\sin^2\tfrac{1}{2}\omega\Delta. \tag{25}$$

Thus taking $\tilde{v} - \tilde{v}''\Delta^2/12$ for the velocity is equivalent to having the filter function

$$\left(\frac{\sin\frac{1}{2}\omega\Delta}{\frac{1}{2}\omega\Delta}\right)^2(1+\tfrac{1}{3}\sin^2\tfrac{1}{2}\omega\Delta)^2. \tag{26}$$

This filter function is also shown in figure 8. It is much closer to the ideal filter than is the original. It overshoots about 10 %, which is acceptable because it reconstitutes virtually everything below $\frac{1}{2}$. This overcompensation scheme, then, was used throughout in estimating particle velocities. Obviously, the smoothed second derivative of the velocity could not be calculated between the first two or last two cameras, but it was calculated elsewhere.

The following analysis is done in order to obtain an idea of the effect of the low sampling rate. Halfway between cameras one and two, the Nyquist frequency is about 92 Hz, the highest frequency with non-negligible energy in the turbulence is thus 46 Hz. This corresponds roughly to the peak of the dissipation spectrum. The spacing between the first two cameras is about 28 msec, giving $f\Delta = 1{\cdot}3$. From figure 8, it is seen that any particle motion at this frequency is lost. However, at this point, the spectrum of the turbulence is very far down. The location of the half-power point of the Lagrangian spectrum may be crudely estimated to be at $f_h\Delta = 0{\cdot}082$, from the model of the Eulerian time spectrum discussed in § 3.5. From figure 8, it is seen that anything below $f\Delta = 0{\cdot}5$ is reconstituted. Since the location of the half-power point of the forcing function (the turbulence) is estimated to be a factor of six lower than the filter cut-off point, the sampling rate can be viewed more optimistically. In addition, the heavy particle time constants are around 50 msec; they have a half-power frequency (in an oscillating Stokes flow) of $f\Delta = 0{\cdot}09$, showing that the heavy particles probably contained negligible energy at frequencies higher than were measured.

Results. The probability densities of the particle positions and velocities were Gaussian, within the limits of experimental scatter. For large times, this is a likely consequence of the random nature of the turbulence. For small times, this is a consequence of the fact that the probability density of the fluid velocity is Gaussian.

Figure 9 shows the particle dispersion curves. As expected, the lighter the particle, the larger is the dispersion. It is to be noted, however, that the hollow glass bead curve has significant curvature whereas the copper bead curve is nearly linear for large times. Thus, it is immediately obvious that the integral

scales for the lighter particle autocorrelations are larger than those for the heavier particles. The dispersions for the glass and copper beads (same time constant) are nearly identical.

The particle velocity decay is compared with the turbulent velocity decay in figure 10. The decay is linear and the virtual origins are the same for the turbulence and all the particles. The fact that the end-points for the particle decay are

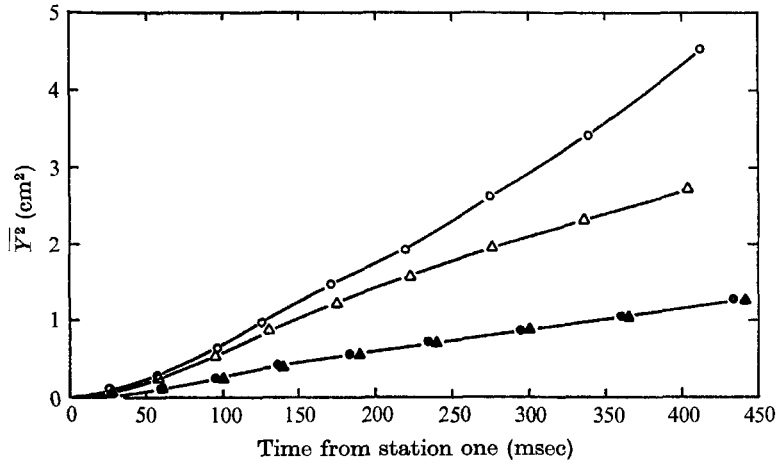

FIGURE 9. Particle dispersion. ○, hollow glass; △, corn pollen; ●, glass; ▲, copper.

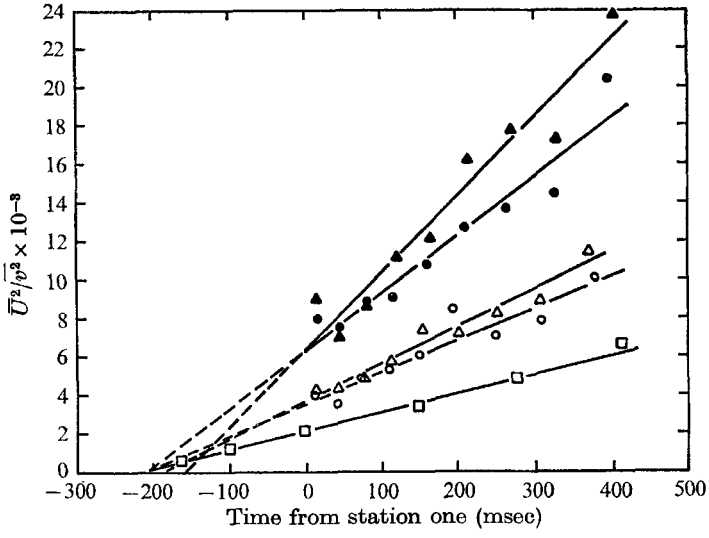

FIGURE 10. Particle velocity decay. ○, hollow glass; △, corn pollen; ●, glass; ▲, copper; □, turbulence.

consistently high with respect to the least-squares linear curve is most likely a consequence of the inability to apply the compensation there. The difference between the velocity of the glass and copper beads is somewhat surprising since their time constants were nearly the same and their dispersion curves were nearly identical. The tread, however, is consistent. The time constant of the copper

beads is slightly larger than that of the glass beads, the velocity is lower, and the dispersion is slightly smaller. It is also seen that the smallest and lightest beads (hollow glass) still do not follow the flow perfectly; if they did their velocities would match that of the turbulence. The difference between the velocities of the glass (or copper) and corn pollen is larger than expected in view of the fact that their time constants differ by only a factor of $2\frac{1}{2}$. The difference between the velocities of the corn pollen and hollow glass beads is surprisingly small when compared, say, with the difference between the velocities of the hollow glass and turbulence, since their time constants differ by a factor of 12. It is likely that a significant portion of the energy of the hollow glass beads was lost due to the low sampling rate. It is easy to show from the oscillating Stokes flow problem that the hollow glass beads would follow even the highest frequency fluctuations of the turbulence. Assuming this to be the case and reasoning from the rather crude model of the Lagrangian spectrum, it is not difficult to show that perhaps as much as 40 % of the energy of the hollow glass beads could have been lost due to the low sampling rate. If this were the case, the velocity of the hollow glass beads would match that of the turbulence. These estimates are rather speculative because the form of the Lagrangian spectrum is unknown.

Another aspect which deserves comment is the fact that the overcompensation scheme appeared to add about the same percentage of energy to all the spectra of particle energies. This was unexpected. One would expect that, if the particles contained negligible energy at frequencies near the cut-off point, the compensation would add negligible energy, whereas, if they contained significant energy, then the compensation would add significant energy. Since it was reasoned previously that the heavy particles would contain negligible energy at the cut-off point, it was expected that the compensation would add negligible energy. Perhaps the explanation is that the noise from the measurement errors was much more significant for the heavier particles. The lower the velocity, the more significant is the measurement error. Also, the measurement error makes its most significant contribution at the highest frequency. It is likely then, that the total of the two effects resulted in the compensation adding nearly the same percentage of energy to the spectra.

Although it is not correct to ascribe all of the difference between the particle and turbulence velocities to the inertia effect, it is intuitive that the particle inertia is the major cause of the difference. As discussed above, it is not certain that the hollow glass beads have a significant inertia effect, in spite of the measurements shown.

Figure 11 shows the decay-corrected autocorrelation functions for the four particle types. It is seen that the solid glass and copper beads have nearly identical autocorrelations; they have nearly the same time constant, but differ by a factor of two in diameter. As expected, the diameter variation plays an insignificant role in this range of length-scale ratios. In comparing all four curves, it is seen that, in marked contrast with Kennedy's (1965) data, the heavy particle correlations decrease much more rapidly than do those for the lighter particles. Kennedy obviously did not realize the significance of the crossing-trajectories effect. He stated "one would certainly expect the solid particle correlation to

remain higher than the fluid particle for all times, simply because of the inertia of the particle". In fact, when he found that the heat wake data showed the opposite effect, he attempted to correct for 'additional molecular diffusion'. When one carefully studies Kennedy's figures, it is very understandable that preconceived ideas of expected behaviour could have influenced the way in which the dispersion curves were drawn and the double-differentiation process. Even a very slight amount of scatter in the dispersion curve can strongly influence the second derivative. The present method, of course, avoided the double-differentiation process.

Although it is not correct to ascribe all of the differences between the correlations to the crossing-trajectories effect, it is intuitive that this effect is the major cause of the difference. The inertia effect would cause an opposite trend.

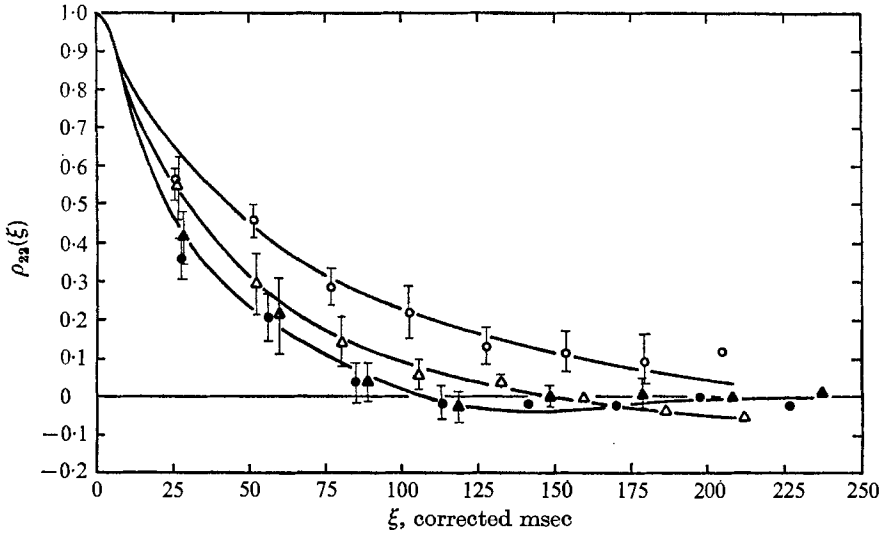

FIGURE 11. Particle velocity autocorrelations. ○, hollow glass; △, corn pollen; ●, glass; ▲, copper. Bars indicate root-mean-square deviation.

As an overall check on the correlations, decay-corrections, compensation scheme, and particle energy data, the correlations and energy decay were fitted with the faired curves shown and a double integration was performed to predict the particle dispersions. Figure 12 shows two examples in which the dispersion predicted by this method is compared with the actual measured dispersion. The agreement is regarded as excellent.

In figure 13, the particle velocity and lateral Eulerian correlations are plotted with the abscissa non-dimensionalized by the respective integral scales. The similarity in shape is striking; it is safe to say that within the limits of experimental error, the particle velocity autocorrelations are similar in shape to the Eulerian spatial autocorrelation. This was the prediction of Yudine's (1959) and Csanady's (1967) theories for heavy particles. It has also been suggested by several authors (see Pasquill 1962, p. 97) that Lagrangian and Eulerian correlations are identical in shape but differ only in time scale, i.e. $\rho_L(\xi) = \rho_E(\beta\xi)$,

where $\beta = T_L/T_E$. Pasquill (1962) suggests a value of $\beta = 4$ based on experiments by Hay & Pasquill (1957). Figure 13 shows that the particle correlations are similar in shape to the Eulerian correlation measured at a fixed point. In this work, if the heavy particle correlations are interpreted as representative Eulerian correlations and light particle correlations as Lagrangian correlations, then $\beta = 3$.

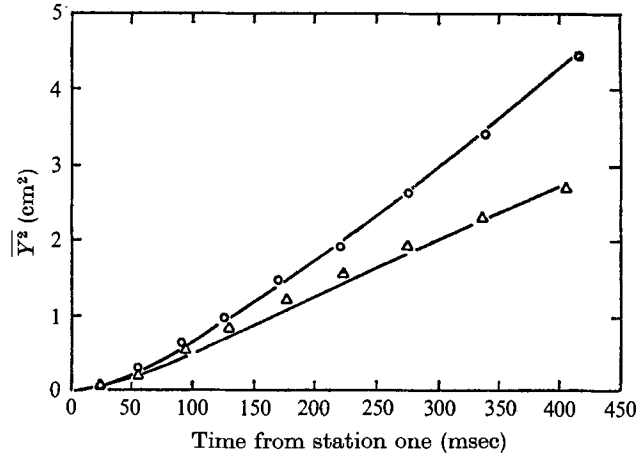

FIGURE 12. Comparison of predicted and measured dispersion. ○, hollow glass; △, corn pollen; ——, double integration of autocorrelations.

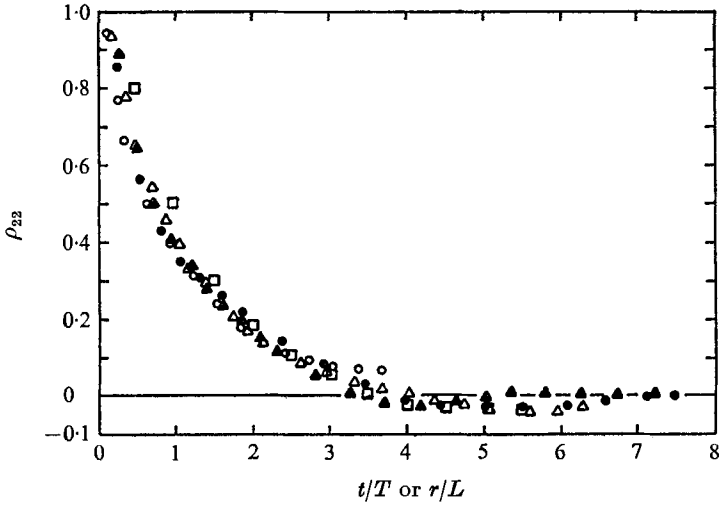

FIGURE 13. Non-dimensional graph of correlations. ○, hollow glass; △, corn pollen; ●, glass; ▲, copper; □, Eulerian spatial.

There is no theoretical reason to expect the correlations shown in figure 13 to be of the same shape. In fact, dimensional reasoning suggests that the Eulerian spatial correlation *cannot* have the same shape as the Lagrangian time correlation. Kolmogoroff's theory shows that $F(\kappa) = \alpha_1 \epsilon^{\frac{2}{3}} \kappa^{-\frac{5}{3}}$ and that $S(\omega) = \alpha_2 \epsilon \omega^{-2}$, so that the spectra, and hence the correlations, cannot have the same shape. Experimentally, it is difficult to measure a difference between the two, as evidenced by

figure 13. From a practical viewpoint, however, this is a fortunate coincidence. The exact shape of the correlation is unimportant; what is most important are the Lagrangian, Eulerian, and particle velocity time integral scales.

Figure 14 shows a graph of particle integral scale versus particle time constant. Although it is difficult to draw firm conclusions, it appears that the curve may be asymptotic to $T_L = 100$ msec as T_p goes to zero. This is, of course, an estimate of the Lagrangian integral scale. At the opposite extreme, the integral scale must go to zero as the particle time constant goes to infinity. In this case, the particle sees a 'frozen' field as it rapidly cuts through the turbulence, and its motion is more adequately described in terms of the Eulerian spatial correlation.

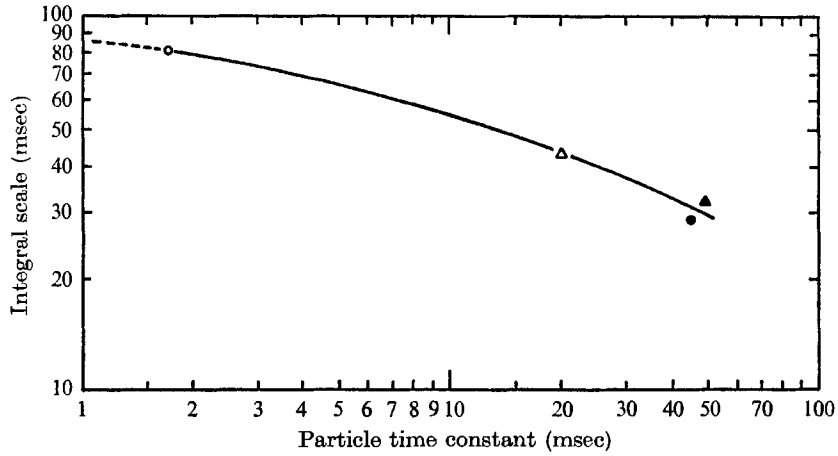

FIGURE 14. Variation of integral scale with particle time constant. ○, hollow glass; △, corn pollen; ●, glass; ▲, copper.

Corrsin (1963*a*) estimated the Lagrangian integral scale to be L/u', where L is the Eulerian spatial integral scale and u' is the root-mean-square turbulence intensity. The lateral integral scale was found to be about 1·2 cm and the turbulence intensity was 13 cm/sec at $x/M = 73$. Hence, this experiment shows Corrsin's estimate to be very close to the true value.

6. Conclusions

Criteria were developed for determining the type of flow, the sampling rate, the number of observations, and the correction accounting for the turbulence decay, which were necessary for making adequate measurements of the autocorrelations. Various sources of error were analyzed; the parallax error was negligible, the particle size variation was unimportant, the film reading errors were negligible, the effect of the replacement of missing pictures was small, and the relative error accompanying the estimate of the autocorrelation from a finite number of measurements was unavoidable.

The wind tunnel generated a homogeneous and isotropic turbulent flow. A method for photographing the small particles was developed. A particle

injector was constructed to launch single particles into the flow at the mean flow speed. A detector determined when a particle had entered the tunnel and a timing system triggered the flashtubes in sequence as the particle entered the field of view of the respective camera. Particle positions were recorded on film; the particle positions were measured and analyzed to determine the autocorrelation functions. The Eulerian properties of the turbulence were measured. The conclusions are: (*a*) The turbulence field is homogeneous in planes perpendicular to the mean flow. (*b*) The energy decay corrections can be made because the flow is self-preserving. (*c*) The probability densities of particle positions are Gaussian. (*d*) The probability densities of particle velocities are Gaussian. (*e*) Within the limits of experimental error, the particle and turbulent velocity decay have the same virtual origin. (*f*) The autocorrelations decrease faster for heavier particles, in marked contrast with previous experimental results. (*g*) All of the particles with the possible exception of the hollow glass beads have significant inertia effects. (*h*) All of the particles with the possible exception of the hollow glass beads have significant crossing-trajectories effect. (*i*) Within the limits of experimental scatter, all of the particle velocity autocorrelations and the Eulerian spatial correlation have similar shapes. (*j*) A crude estimate showed the ratio of Eulerian to Lagrangian time scales to be 3. (*k*) The Lagrangian integral scale is closely approximated by L/u'.

This paper is a condensed version of a thesis with the same title submitted by one of the authors (W.H.S.) to the Pennsylvania State University for the degree of Doctor of Philosophy. The authors are grateful to Dr Hendrik Tennekee for his consultations during various phases of the study, to Mr Thomas Gatski for his skillful assistance, and to Mr Robert Pierce for his help with the electronics. The authors gratefully acknowledge the financial support of the U.S. Army under contract DAAA-15-67-C-0620.

REFERENCES

Baines, W. D. & Peterson, E. G. 1951 *Trans. ASME* **73**, 467–480.

Batchelor, G. K. 1952 *Proc. Camb. Phil. Soc.* **48**, 345–362.

Batchelor, G. K. 1956 *The Theory of Homogeneous Turbulence.* Cambridge University Press.

Batchelor, G. K. 1957 *J. Fluid Mech.* **3**, 67–80.

Batchelor, G. K. & Townsend, A. A. 1948 *Proc. Roy. Soc.* A **193**, 539–558.

Batchelor, G. K. & Townsend, A. A. 1956 *Surveys in Mechanics.* Cambridge University Press.

Champagne, F. H. & Sleicher, C. A. 1967 *J. Fluid Mech.* **28**, 177–182.

Champagne, F. H., Sleicher, C. A. & Wehrmann, O. H. 1967 *J. Fluid Mech.* **28**, 153–175.

Comte-Bellot, G. & Corrsin, S. 1966 *J. Fluid Mech.* **25**, 657–682.

Corrsin, S. 1963*a* *J. Atmos. Sci.* **20**, 115–119.

Corrsin, S. 1963*b* *Handbuch der Physik*, **8**, 524–590.

Corrsin, S. & Lumley, J. L. 1956 *Appl. Sci. Res.* A **6**, 114–116.

Csanady, G. T. 1963 *J. Atmos. Sci.* **20**, 201–208.

Csanady, G. T. 1964 *J. Atmos. Sci.* **21**, 222–225.

Csanady, G. T. 1967 Rep. no. 4, Contract DA-18-035-AMC-399(A), vol. 2, The Travelers Research Center, Hartford, Conn.

FRENZEN, P. 1963 *Argonne National Lab.* A.N.L.-6794.

FUCHS, N. A. 1964 *The Mechanics of Aerosols.* Macmillan.

GRANT, H. L. & NISBET, I. C. T. 1957 *J. Fluid Mech.* **2**, 263–272.

HAY, J. S. & PASQUILL, F. 1957 *J. Fluid Mech.* **2**, 299–310.

INOUE, E. 1951 Unpublished, Geophy. Inst., Univ. of Tokyo.

KÁRMÁN, T. VON & HOWARTH, L. 1938 *Proc. Roy. Soc.* A **164**, 192–215.

KENNEDY, D. A. 1965 Ph.D. Dissertation, Dept. of Mechanics, The Johns Hopkins University.

LIN, C. C. 1961 *Statistical Theories of Turbulence.* Princeton University Press.

LUMLEY, J. L. 1957 Ph.D. Dissertation, Dept. of Mechanics, The Johns Hopkins University.

LUMLEY, J. L. 1960 *Appl. Sci. Res.* A **10**, 153–157.

LUMLEY, J. L. & CORRSIN, S. 1959 Proc. Int. Symp. of Atmos. Diff. and Air Poll. *Advances in Geophysics*, **6**, 179–183.

LUMLEY, J. L. & PANOFSKY, H. A. 1964 *The Structure of Atmospheric Turbulence.* Interscience.

LUMLEY, J. L. & SNYDER, W. H. 1968 Quarterly Progress Report no. 2, Dept. of Aero. Engr., The Pennsylvania State University.

MICKELSEN, W. R. 1960 *J. Fluid Mech.* **7**, 397–400.

MONIN, A. S. & YAGLOM, A. M. 1965 *Statistical Hydromechanics, The Mechanics of Turbulence*, Part 1. Moscow: Nauka Press.

OKUBO, A. 1967 *Phys. Fluids Suppl.* **10**, S 72–75.

PASQUILL, F. 1962 *Atmospheric Diffusion.* Van Nostrand.

PATTERSON, G. S. & CORRSIN, S. 1966 *Dynamics of Fluids and Plasmas.* Academic.

SAFFMAN, P. G. 1960 *J. Fluid Mech.* **8**, 273–283.

SAFFMAN, P. G. 1961 *La Mechanique de la Turbulence*, pp. 53–62. Paris: C.N.R.S.

SHIRAZI, M. A., CHAO, B. T. & JONES, B. G. 1967 Report, University of Illinois at Urbana.

SNYDER, W. H. 1969 Ph.D. Dissertation, Dept. of Aerospace Engr., The Pennsylvania State University.

SUTTON, O. G. 1947 *Quart. J. Roy. Met. Soc.* **73**, 426–436.

TAYLOR, G. I. 1921 *Proc. Lond. Math. Soc.* **20**, 196–211.

TAYLOR, G. I. 1935 *Proc. Roy. Soc.* A **151**, 421–478.

TENNEKES, H. & LUMLEY, J. L. 1971 *A First Course in Turbulence.* Prentice Hall.

TCHEN, C. M. 1947 Ph.D. Dissertation, University of Delft (Martinus Nijhoff, The Hague).

TOWNSEND, A. A. 1954 *Proc. Roy. Soc.* A **224**, 487–512.

VANONI, V. A. & BROOKS, N. H. 1955 Cal. Inst. Tech., Rep. no. E-46 (ASTIA Reprint Ad 66182).

WELFORD, W. T. 1962 *Proc. of Conf. on Optical Inst.* London: Chapman and Hall.

WYNGAARD, J. C. 1968 *J. Scient. Instrum.* Ser. 2, **1**, 1105–1108.

WYNGAARD, J. C. & LUMLEY, J. L. 1967 *J. Scient. Instrum.* **44**, 363–365.

YUDINE, M. I. 1959 Proc. Int. Symp. on Atmos. Diff. and Air. Poll. *Advances in Geophysics*, **6**, 185–191.